Journal of Hydrospace Technology, Vol. 1, No. 2, 1995, pp. 83-99

Application of a Potential-Based Panel Method for Analysis of a Two-Dimensional Cavitating Hydrofoils Advancing Beneath a Free Surface

Jae-Moon Lew* , Chang-Sup Lee* and Young-Gi Kim†

Abstract

A potential-based panel method is presented for the analysis of a partially or supercavitating two-dimensional hydrofoil at a finite submergence beneath a free surface, treating without approximation the effects of the finite Froude number and the hydrostatic pressure.

Free surface sources and normal dipoles are distributed on the foil and cavity surfaces, their strength being determined by satisfying the kinematic and dynamic boundary conditions on the foil-cavity boundary. The cavity surface is determined iteratively as a part of the solution.

Numerical results show that the wave profile is altered significantly due to the presence of the cavity. The buoyancy effect due to the hydrostatic pressure, which has usually been neglected in most of the cavitating flow analysis, is found playing an important role, especially for the supercavitating hydrofoil; the gravity field increases the cavity size in shallow submergence, but decreases when deeply submerged, while the lift is reduced at all depth.

1 Introduction

Recently the need for a fast ship is increasing not only for the military purpose but also for the transportation of passengers and modern commercial products.[1] Hull forms of new concept are now under investigations, the hydrofoil being considered a useful means producing lift in many cases. At high speed it is impossible to avoid the cavitation on and around the hydrofoil, and hence we should be able to predict with a sufficient accuracy such behavior of cavity as the inception, the extent and the shape, for the proper design of hydrofoils.

Researches on the cavity around the body were initiated by Helmholtz in 1868 and Kirchoff in 1869 by the hodograph method. Then in 1907 Levi-Civita extended the method for the flow around the curved obstacle. The first engineering application of these works was made possible half a century later by Tulin[2] for the analysis of the supercavitating

*Member, Chungnam National University

†Member, Chungnam National University; Presently at Samsung Heavy Industries Co. Ltd

flow, and followed by numerous investigations (see, for example, Tulin[2] for the review of general papers related to the cavity flow).

Analysis on the cavitation in practice is carried out under various assumptions. The fluid is assumed incompressible, inviscid and irrotational. The angle of attack, the cavity thickness and the wave amplitude are assumed small to enable the linearization. The cavity termination condition has to be suitably specified. The influence of the hydrostatic pressure term in the cavitating free surface wave analysis has usually been neglected. Our aim is to analyze the cavity flow past a hydrofoil, advancing with a finite Froude number, and at the same time to show the importance of the buoyancy effect, that is, the gravity effect on the submerged foil-cavity system, in the cavity analysis. We therefore review the existing papers in three categories as follows:

- Literature where the buoyancy effect in unbounded fluid is neglected.
- Literature where the buoyancy effect in unbounded fluid is considered.
- Literature where the buoyancy effect in a free surface flow is neglected.

Linear theory for the first category was typically developed by Geurst[3] and Tulin[2] under the assumption that the thickness of the body and the cavity is small compared to the dimension of the body in the main stream direction. Nonlinear analysis was carried out analytically by Wu[4] for the supercavitating flow of infinite cavity length. Numerical analysis to solve the integral equation, formulated based on Green's identity, was first performed by Golden[5], using the discrete vortex/source distribution method for the two-dimensional hydrofoil. This was extended to the supercavitating hydrofoil of the finite span by Jiang[6] and further to the unsteady cavitating propeller by Lee[7], enabling the prediction of cavity extent and volume variation. Analysis up to this point was based on the linear theory. Nonlinear analysis considering the exact cavity and hydrofoil thickness was done by Uhlman[8][9] for the two-dimensional hydrofoil in partially- and supercavitating conditions by the method of vorticity distribution. A new nonlinear boundary element method based on the potential formulation is recently reported by Lee[10],[11] Kim et al[12] and Kinnas and Fine[13].

The effect of the transverse gravity field, that is, the buoyancy effect, upon the cavity flow in unbounded fluid was first considered by Street[15][14]. He solved the linearized supercavitating flow around a symmetric wedge section, including the hydrostatic pressure, and found that the gravity effect produces the negative lift in the supercavitating flow. Kiceniuk and Acosta[16] then verified the results experimentally. By applying the conformal mapping technique, Larock and Street[17] developed a nonlinear theory and solved a mixed-boundary-value-problem to find that the gravity effect reduces the lift and cavity size. In their analysis they adopted the single spiral model, which permits the sudden velocity jump at the cavity termination point (see Tulin[2] for description of the termination modelings).

The cavity flow beneath a free surface has been dealt with many authors. In early sixties, linear theories were developed treating single flat-plate hydrofoil with a finite cavity near the free surface (see, for example, Yim[18]), and Green and Street[19] subsequently treated by the linear theory two supercavitating hydrofoils of finite cavity length at infinite

Froude number. Larock and Street[20] also analyzed the supercavitating flow past a two-dimensional flat plate by using Riemann-Hilbert mapping technique. They treated the finite cavity length problem and adopted the double-spiral cavity termination model. For the hydrofoil of arbitrary section, Furuya[21] applied the nonlinear theory and solved the problem in an iterative manner. It should be noted that the works up to this point are all carried out for the infinite Froude number flow, neglecting the buoyancy effect. Applying Green's theorem, Doctors[22] recently introduced the method of the free surface source distribution on the body and cavity surfaces for the hydrofoil advancing at a finite Froude number. Although he could satisfy the linearized free surface condition, the radiation condition and the infinite depth bottom boundary condition by using the Kelvin sources, he suffered from a numerical difficulties in his velocity-based formulation, and had to resort to the least square fitting method to remove the highly oscillating behavior of the source strength along the cavity surface. He also neglected the buoyancy effect, while dealing with the finite Froude number problem.

In the present study, we treat the partially- or supercavitating flow past a two-dimensional hydrofoil advancing under a free surface with a finite Froude number. We applied Green's identity to derive the integral equation for the unknown velocity potential on the foil and cavity surfaces. By introducing the free surface dipoles and sources, we satisfy the linearized free surface condition and the radiation condition at the outset. We include the hydrostatic pressure term in evaluating the dynamic condition on the cavity surface and show the significance of this buoyancy effect.

2 Statement of the Boundary Value Problem

Let's consider a two-dimensional cavitating hydrofoil placed in an inviscid, incompressible and irrotational fluid. A Cartesian coordinate system is chosen as shown in Figure 1, with the x-axis placed on the undisturbed free surface, S_F, and with the positive y-axis pointing the opposite of the gravitational acceleration. The hydrofoil of the chordlength c is inclined by an angle of attack α relative to the uniform oncoming free stream in the positive x-direction. The leading edge of the foil is located at $x = 0$ and below the undisturbed free surface at $y = -d$, d being the submergence.

The total velocity, $\underline{V}$, may be expressed in terms of the total velocity potential, Φ, which is defined using the oncoming velocity, $\underline{U}_\infty$, the position vector, $\underline{x}$, and the perturbation potential, ϕ, as follows:

$$\underline{V} = \nabla\Phi \tag{1}$$

where

$$\Phi = \underline{U}_\infty \cdot \underline{x} + \phi \tag{2}$$

Conservation of the mass applied to the potential flow gives the Laplace equation valid in the fluid region as a governing equation:

$$\nabla^2\Phi = 0 \tag{3}$$

We assume that the amplitude of the free surface, ζ_w, or the disturbance is small so that the boundary condition on the free surface may be linearized. Motion of the fluid can be uniquely defined by imposing the boundary conditions on the boundary surfaces as follows:

1. Linearized free surface condition on the free surface S_F:

$$\Phi_{xx} + \nu\Phi_y = 0 \tag{4}$$

where $U_\infty = |\underline{U}_\infty|$ and $\nu = g/U_\infty^2$. The free surface elevation on the free surface S_F may be expressed as

$$\zeta_w = -\frac{U_\infty}{g}\phi_x \tag{5}$$

2. Radiation condition at infinity upstream and downstream:

$$\lim_{x\to-\infty} |\nabla\Phi| = |\underline{U}_\infty| \,, \quad \text{and} \quad \lim_{x\to+\infty} |\nabla\Phi| < \infty \tag{6}$$

3. Flow tangency condition on the body surface S_B:

$$\hat{n} \cdot \underline{V} = \frac{\partial\Phi}{\partial n} = 0 \tag{7}$$

where $\hat{n}$ is the unit vector normal to the boundary, defined positive when pointing into the fluid region.

4. Quiescence condition at infinite depth:

$$\lim_{y\to-\infty} \nabla\Phi \to \underline{U}_\infty \tag{8}$$

5. Kutta condition at the trailing edge:

$$|\underline{V}_{T.E.}| < \infty \tag{9}$$

where $T.E.$ stands for the trailing edge.

For the partially cavitating flow, the Kutta condition requires that the magnitude of the velocity be finite at the trailing edge as in the subcavitating flow. The same condition may, however, be implemented in a different way for the supercavitating case, since the trailing edge is the junction point of the two distinct flow regions. The Kutta condition may be restated that the flow across the trailing edge be smooth and continuous. See Lee et al[11] and Wu[4][23] for additional description of the requirement at the junction point, that is, the detachment condition at either the leading or the trailing edges.

With the presence of cavity around the hydrofoil, we have to apply the kinematic and dynamic boundary conditions on the cavity surface, the cavity closure condition at the cavity trailing end and the cavity detachment condition.

6. Kinematic condition on the cavity surface S_C:

$$\frac{DF}{Dt} = 0 \tag{10}$$

where $F(x, y)$ is a function expressing the cavity surface.

7. Dynamic condition on the cavity surface S_C:

$$p = p_v \tag{11}$$

where p_v is the vapor pressure inside the cavity.

8. Cavity closure condition at the cavity trailing end:

$$T^c(x_{cte}) = 0 \tag{12}$$

where $T^c(x)$ denotes the cavity thickness function and x_{cte} denotes the x-coordinate of the cavity trailing end.

9. Detachment condition at the trailing edge of the foil in supercavitating flow is the continuity of the velocity vectors at the trailing edge:

$$\lim_{A \to T.E.} \underline{V}_A = \lim_{B \to T.E.} \underline{V}_B \tag{13}$$

where A and B are points positioned on the lower part of the hydrofoil and cavity surfaces connected at the trailing edge, respectively.

Using the Bernoulli equation, we get relations between the surface pressure, p, the tangential speed on the foil-cavity surface, $|\underline{V}_t|$, the cavitation number, σ, and the pressure coefficient, C_p, as follows:

1. Case when the buoyancy effect is not included:

$$C_p \equiv \frac{p - p_\infty}{\frac{1}{2}\rho U_\infty^2} = 1 - (\frac{|\underline{V}_t|}{U_\infty})^2 , \quad \text{on foil/cavity surface} \tag{14}$$

$$\sigma \equiv \frac{p_\infty - p_v}{\frac{1}{2}\rho U_\infty^2} = -C_{p_v} = (\frac{|\underline{V}_c|}{U_\infty})^2 - 1 , \quad \text{on the cavity surface} \tag{15}$$

where ρ is the density of water, p_∞ is the ambient pressure at the depth of the leading edge upstream infinity, that is, $p_\infty = p_{atm} + \rho g d$, p_{atm} being the atmospheric pressure, and $|\underline{V}_c|$ is the tangential speed on the cavity surface.

2. Case when the buoyancy effect is included:

$$C_p \equiv \frac{p - p_\infty}{\frac{1}{2}\rho U_\infty^2} = 1 - (\frac{|\underline{V}_t|}{U_\infty})^2 - \frac{2(y - y_{ref})/c}{F_c^2} \tag{16}$$

$$\sigma \equiv \frac{p_\infty - p_v}{\frac{1}{2}\rho U_\infty^2}$$

$$= -C_{p_v} = (\frac{|\underline{V}_c|}{U_\infty})^2 - 1 + \frac{2(y_c - y_{ref})/c}{F_c^2} , \quad \text{on the cavity surface} \tag{17}$$

where c the chordlength, y_c and y_{ref} the y-coordinates of the cavity surface and the leading edge, respectively, and $F_c = U_\infty / \sqrt{gc}$ the Froude number of the oncoming flow.

In this paper, we are interested in the lift, L, the drag, D, and the moment, M, acting on the hydrofoil in cavitating condition and also the cavity volume, Vol (or, the cavity section area in the present two-dimensional problem).

The nondimensional coefficients of these quantities are defined following the expression of Uhlman[8].

The lift coefficient, C_L, is given as

$$C_L \equiv \frac{L}{\frac{1}{2}\rho U_\infty^2 c} = -\oint_{S_B} C_p \hat{t} \cdot \frac{U_\infty}{U_\infty} ds \tag{18}$$

the drag coefficient, C_D, is

$$C_D \equiv \frac{D}{\frac{1}{2}\rho U_\infty^2 c} = -\oint_{S_B} C_p \hat{n} \cdot \frac{U_\infty}{U_\infty} ds \tag{19}$$

and the moment coefficient, C_M, about the leading edge of the hydrofoil is

$$C_M \hat{k} \equiv \frac{M\hat{k}}{\frac{1}{2}\rho U_\infty^2 c^2} = -\oint_{S_B} C_p \underline{r} \times \hat{n}\, ds \tag{20}$$

where c denotes the chordlength and $\underline{r}$ denotes a vector from the leading edge to a point on the foil surface; $\hat{t}$ is the unit tangential vector defined in the clockwise direction along the foil surface as shown in Figure 1, and $\hat{k}$ is the unit vector normal to the $x-y$ plane.

The cavity volume, Vol, is calculated from the cavity thickness function, $T^c(x)$, as

$$Vol = \int_0^{\ell_{cav}} T^c(x)\, dx \tag{21}$$

where ℓ_{cav} is the cavity length defined along the x-axis as shown in Figure 1. For super-cavitating flow, $T^c(x)$ becomes the vertical extent of the upper and lower cavity surfaces.

3 Singularity Distribution Method

To treat the cavitating flow under a free surface, we may derive an expression for the potential in the flow field by distributing the free surface dipoles and sources on the body surface.

The total potential in the fluid region may now be expressed as follows:

$$\begin{aligned}\Phi(\underline{x}) = U_\infty x \;+\; & \int_{S_B \cup S_C} \frac{\mu(\underline{\xi})}{2\pi} \frac{\partial}{\partial n_\xi} G(\underline{x};\underline{\xi})\, dS \\ + \; & \int_{S_C} \frac{q(\underline{\xi})}{2\pi} G(\underline{x};\underline{\xi})\, dS + \int_{S_w} \frac{\mu_w}{2\pi} \frac{\partial}{\partial n_\xi} G(\underline{x};\underline{\xi})\, dS\end{aligned} \tag{22}$$

where

$$
\begin{aligned}
q(\underline{\xi}) &= \text{free-surface source strength} \\
\mu(\underline{\xi}) &= \text{free-surface normal dipole strength} \\
\underline{x}(x,y) &= \text{field point where the induced potentials are calculated, } (x+iy) \\
G(\underline{x};\underline{\xi}) &= \ln(\underline{x}-\underline{\xi}) + \ln(\underline{x}-\underline{\xi}') + 2\int \frac{e^{-ik(\underline{x}-\underline{\xi}')}}{k-\nu}dk - 2\pi i e^{-i\nu(\underline{x}-\underline{\xi}')} \\
\frac{\partial}{\partial n_\xi} &= \text{normal derivative with respect to the point } \underline{\xi} \\
\underline{\xi}(\xi,\eta) &= \text{point where the singularity is located, } (\xi+i\eta) \\
\underline{\xi}'(\xi,\eta) &= \text{complex conjugate of } \underline{\xi}, \ (\xi-i\eta)
\end{aligned}
$$

and also S_B, S_C and S_w denote the body surface, the cavity surface and the wake sheet surface, respectively, and μ_w denotes the dipole strength on the wake sheet surface, S_w, which is negative of the jump of potentials across the wake sheet surface. The direction of the dipole in the wake sheet surface, S_w, is defined positive when pointing upward.

For dipole only distribution, we may convert the flow tangency condition (7), $\partial\Phi/\partial n = 0$, in the fluid side of the boundary into the zero total potential condition, for the fictitious internal flow,

$$\Phi^-(\underline{x}) = 0 \tag{23}$$

where the superscript denotes that the velocity potential is to be calculated on the interior to the foil surface.

Equation (22) may now be reformed and applied to a point on and inside the foil-cavity surface to meet the alternative form of the kinematic boundary condition (23) as

$$
\begin{aligned}
\Phi^-(\underline{x}) = 0 = U_\infty x \ &+ \ \frac{\mu(\underline{x})}{2} + \int\!\!\!\!\!\!- _{S_B \cup S_C} \frac{\mu(\underline{\xi})}{2\pi}\frac{\partial}{\partial n_\xi}G(\underline{x};\underline{\xi})\,dS \\
&+ \int_{S_C}\frac{q(\underline{\xi})}{2\pi}G(\underline{x};\underline{\xi})\,dS + \int_{S_w}\frac{\mu_w}{2\pi}\frac{\partial}{\partial n_\xi}G(\underline{x};\underline{\xi})\,dS
\end{aligned} \tag{24}
$$

In case of partially cavitating flow, μ_w is the negative of the potential jump at the trailing edge, whereas, in fully cavitating flow, μ_w is that at the cavity trailing end.

From the dynamic boundary condition and equations (16) and (17), the hydrostatic pressure relates the speed on the cavity surface $|\vec{V}_t|$ with the Froude number and the cavity thickness. If we express the speed on the cavity as a product of the reference speed $|\vec{V}_t|_{cle}$ and a correction factor function dependent upon the streamwise position $a(s)$, that is, $|\vec{V}_t| = a(s)|\vec{V}_t|_{cle}$, the strength of the dipole on the cavity surface may be expressed as:

$$
\begin{aligned}
\mu(\vec{\xi}) &= -\{\Phi^+(\vec{\xi}) - \Phi^-(\vec{\xi})\} = -\{\Phi^+_{cle} + |\vec{V}_t|_{cle}\int_{cle}^{\vec{\xi}} a(s)ds\} \\
&= \mu_{cle} - |\vec{V}_t|_{cle}\int_{cle}^{\vec{\xi}} a(s)ds
\end{aligned} \tag{25}
$$

where Φ^+_{cle} and μ_{cle} denote the total potential and the dipole strength at the cavity leading edge, respectively. Equation (25) gives a very useful relation between the tangential speed

on the cavity leading edge $|\vec{V}_t|_{cle}$ and the the dipole strength $\mu(\vec{\xi})$ on the cavity surface. If we neglect the influence of the hydrostatic pressure, (25) degenerates into a simple linear relation since $a(s) = 1$. On the other case of the varying hydrostatic pressure, the correction factor $a(s)$, which is dependent upon the unknown cavity surface location, should be computed iteratively. The iteration procedure is however very stable and fast since the correction function is close to 1 and only depends on the small variation of the transverse extent of the cavity surface.

The source strength representing the thickness of the cavity or, more correctly, the function to relocate the current cavity surface position in an iterative process may be related, in a linearized sense, to the product of the oncoming velocity and the first derivative of cavity thickness correction function, t^c, as in the case of thin wing theory,

$$q = V_n = U_\infty \frac{dt^c}{dx} \tag{26}$$

$$t^c = T^c_{(i)} - T^c_{(i-1)} \tag{27}$$

where V_n is the normal component of the total velocity on the cavity surface, which is expected to be nonzero when the tangency boundary condition (7) is replaced by the zero total potential condition (23), and the subscript (i) denotes the iteration index. Equation (27) shows that t^c is the difference of the cavity surfaces between two successive iterations. Note that the source strength, $q(\underline{\xi})$, vanishes upon convergence.

Since the cavity thickness, T^c, is to satisfy the closure condition (12), the thickness correction function, t^c, should also satisfy the same condition. Integrating (26), we get expressions for the cavity thickness correction and an alternative form of the cavity closure condition as follows:

$$t^c(l) = \int_0^l \frac{q}{U_\infty} dx \tag{28}$$

$$t^c(\ell_{cav}) = \int_0^{\ell_{cav}} \frac{q}{U_\infty} dx = 0 \tag{29}$$

Once the equation (24) is solved, the cavity source strengths, $q(\underline{\xi})$, are known, and hence the new cavity shape may be obtained by correcting the ordinate of the cavity surface at the current iteration, as schematically shown in Figure 2.

4 Numerical Calculations and Discussions

4.1 Non-cavitating free surface flow

The present paper is the outgrowth of Lee et al[11], who applied the present method to the cavitating flow past a hydrofoil advancing in an unbounded fluid. The numerical procedure are described in detail and evaluated in Lee et al[11] for the case of the unbounded fluid.

The first step in validating the present numerical procedure is, therefore, to analyze the flow past a hydrofoil advancing beneath a free surface in non-cavitating condition. We selected a 12% thick Joukowski section, for which a numerical result by Bai[24]

and experimental data are available. Figure 3 shows the pressure distribution around this Joukowski hydrofoil under the condition of $\alpha = 5$ deg, $F_c = 0.617$, and the leading edge submergence $d/c = 0.113$, together with the comparison with existing data. It is shown that the result correlates well at least with existing numerical methods for the fluid of infinite depth.

4.2 Supercavitating flow

To show the effect of the transverse gravity field upon the cavitating flow, we selected a symmetric wedge placed horizontally in uniform flow. Figure 4 shows the computed (negative) lift, L, non-dimensionalized with the displaced weight of the wedge, B, versus the cavity length relations for the wedge with apex angles, $\beta = 1$ deg and $\beta = 7.5$ deg, together with the linear theoretical result of Street[15] and experiments of Kiceniuk and Acosta[16]. It is first of all observed that the magnitude of the negative lift, that is, the loss of the lift, increases with the increase of the cavity length. It is shown that, for the small apex angle, $\beta = 1$ deg, the computed result ($- \cdot -$) falls on the theoretical line of Street (——) up to the cavity length, $\ell_{cav}/c = 2.0$. The two results deviate from each other, from $\ell_{cav}/c = 2.0$ and above, showing the evidence of the blockage effect upon the lift force of the long buoyant cavity.

Kiceniuk and Acosta[16] carried out experiments with a symmetric $\beta = 7.5$ deg wedge for three Froude numbers, $F_c = 5.0, 6.2$ and 7.5, and their results are reproduced in Figure 4. Our computational results for the same condition are also added in Figure 4, showing little dependency upon Froude number variation. It is noted that the experimental results scatter considerably, which indicates the unsteadiness of the high speed flow condition, while showing the similar trend as the present computation. Figure 5 shows the results for the apex angle, $\beta = 15$ deg, for the same Froude numbers. Deviation between the experiments and the numerical computation increases, which indicates that the wall blockage effect appears more significant with the increase of the apex angle and the transverse thickness of the cavity.

Another computation is made for the flow past a flat plate deeply submerged beneath a free surface, but unlike the existing results such as Lee et al[11], including in the present study the hydrostatic pressure variation due to the gravity in the vertical direction. Figure 6 show the cavity shapes, predicted by considering or without considering the buoyancy effect, for the assumed cavity length, $\ell_{cav}/c = 4.4$. For the same cases with pre-assigned cavity length, the computed lift, drag coefficients and the computed cavitation number, σ, and the cavity volume are compared in Table 1. It may be noted that, for this deeply submerged case, the lift and the cavity size are reduced slightly, although not significant, due to the transverse gravity field variation around the foil and cavity boundary as predicted by Larock and Street[17].

Up to now, the influence of the free surface boundary in contact with the atmosphere is not considered, that is, the effect of the free wave upon the flow around the hydrofoil has been neglected. To the authors' knowledge, there is no published evidence dealing with the transverse gravity effect upon the cavity flow past a hydrofoil advancing at a finite Froude number near a free surface, and hence only the results of the present method will

Table 1: Comparison of the lift, drag coefficients, the cavitation number and cavity volume coefficients, predicted with and without considering the buoyancy effect, for a prescribed cavity length, $\ell_{cav}/c = 4.4$. $N^D = 190$.

	Without buoyancy effect	With buoyancy effect
C_L	0.324	0.307
C_D	0.057	0.054
σ	0.190	0.174
Vol	1.240	1.203

be presented. Figure 7 shows that, for the similar condition as Figure 6 except the finite submergence depth, $d/c = 0.53$, the cavity shape and wave profile are altered significantly. When the hydrostatic pressure term is considered into computation, the position of the cavity upper surface near the leading edge is lowered compared to the surface obtained without considering the gravity effect, but the cavity turns slightly upwards downstream due to the buoyancy effect. Remember that the pressure constant dynamic boundary condition on the cavity surface is equivalent to requiring the velocity being constant when neglecting the buoyancy effect, but on the contrary with the buoyancy effect, the tangential speed on the cavity surface is no longer constant. The tangential speed on the upper surface is less than the speed on the lower surface due to the difference in the hydrostatic pressure. Moreover, the effect is more significant on the upper cavity surface than on the lower surface. It is expected, therefore, that the wave pattern will be influenced to the same degree and should be analyzed with the buoyancy effect into consideration.

We, then, carried out a parametric study to see the influence of the submergence depth and Froude number. Figure 8 shows the cavity volume, the cavity length, and the lift and drag coefficients variations as a function of the cavitation number for three depth conditions, that is, $d/c = 0.5, 1.0$ and 2.0, for a flat-plate hydrofoil at $\alpha = 10$ deg and $F_c = 3.0$. Figure 9 also shows the similar quantities for the same hydrofoil at $\alpha = 10$ deg and the submergence depth, $d/c = 1.0$, for three Froude numbers, that is, $F_c = 3.0, 4.0$ and 5.0. In both figures, the results obtained with or without considering the hydrostatic pressure term in computations are compared. It is noted that the buoyancy effect, due to the depth difference between the upper and lower cavity surfaces, appears most significantly in the cavity volume and the cavity length. At the same cavitation number, by including the buoyancy effect, the cavity volume and the cavity length are reduced when the submerged depth is large, roughly when $d/c > 1.0$, in a similar manner as we observed for the deeply submerged hydrofoil, whereas the trend is reversed for the case of shallow submergence. The lift and drag coefficients decrease at most of the submerged depths when the buoyancy effect is considered.

From Figure 9, we may observe that the buoyancy effect decreases with increase of Froude number, as expected from (16) and (17). The buoyancy effect appears most pronounced at lower Froude numbers when the hydrofoil advances at shallow draft, when $d/c = 1.0$, contrary to the negligible influence for the cavity flow in deeply submerged

Table 2: Buoyancy effect upon the lift and drag coefficients and the cavity length and volume coefficients for a supercavitating hydrofoil at $\alpha = 10$ deg and $d/c = 1.0$ for two Froude numbers, $F_c = 2.0$ and 3.0. Comparison with the non-cavitating case is given.

		Without buoyancy effect	With buoyancy effect	Non-cavitating condition
$F_c = 2.0$ $\sigma = 0.148$	C_L	0.296	0.292	0.665
	C_D	0.052	0.051	0.107
	ℓ_{cav}/c	3.042	2.570	N/A
	Vol	0.563	0.467	N/A
$F_c = 3.0$ $\sigma = 0.142$	C_L	0.313	0.303	0.725
	C_D	0.055	0.053	0.115
	ℓ_{cav}/c	3.081	3.042	N/A
	Vol	0.694	0.677	N/A

condition.

The most noticeable consequence of including the hydrostatic pressure in the computation may be evidenced from Figure 10, which shows the change of the wave elevation for different cavitating conditions. A flat-plate hydrofoil is operating at $\alpha = 10$ deg and $d/c = 1.0$ for two Froude numbers, $F_c = 2.0$ and 3.0. Added together in the figure is the wave elevation generated by a symmetric hydrofoil with 1 % thick biconvex foil section. It may be seen that the wave elevation decreases in general with inclusion of the buoyancy effect, presumably due to the cushioning effect of the constant pressure cavity.

The lift and drag coefficients and the cavity length and volume coefficients obtained for the corresponding cases to Figure 10 are summarized in Table 2. We observe that the buoyancy effect is the same as we have seen in the parametric study. Table 2 also shows that due to the buoyancy effect the lift and the cavity volume reduced by $1.4 \sim 3\%$ and about 20%, respectively, for both Froude number cases.

4.3 Partially-cavitating flow

A computation is made for a partially-cavitating hydrofoil with an NACA 16-006 section advancing at Froude number, $F_c = 0.5$, with $\alpha = 5.0$ deg beneath a free surface at $d/c = 0.6$. Figure 11 shows the cavity shape and the wave profile for the assumed cavity extent of $\ell_{cav}/c = 0.5$, together with the wave pattern generated when the cavity is absent. It is observed that the wave amplitude increases considerably compared to the non-cavitating case, due to the additional thickness effect of the cavity. It is also seen that the cavity and wave profiles, with and without considering the buoyancy effect, are indistinguishable in the partially cavitating case. This is due to the small cavity size and also due to the relatively large Froude number compared to the supercavitating case.

5 Conclusions

A potential-based boundary element method is presented for the analysis of a super- or partially-cavitating two-dimensional hydrofoil advancing at a finite submergence beneath a free surface, treating without approximation the effects of the finite Froude number and the hydrostatic pressure.

- Numerical results show that the wave profile is altered significantly due to the presence of the cavity. The buoyancy effect due to the hydrostatic pressure, which has usually been neglected in most of the cavitating flow analysis, is found playing an important role, especially for the supercavitating hydrofoil.
- At shallow submergence, the cavity length beyond the super-cavitating foil gets longer due to the gravitation effect, which becomes less influential with the increase of the submergence. At shallower submergence, both the lift and drag increase.
- With the increase of the submergence depth and the Froude, the influence of the hydrostatic pressure decreases.
- The hydrostatic pressure effect is negligible for the case of the partially cavitating flow.

The present potential-based boundary element method, developed for the two-dimensional case, may be extended for the analysis of the three-dimensional lifting hydrofoil by replacing the free surface Green function without any difficulty.

References

[1] Holden, K.O., Faltinsen, O. & Moran, T., "Proceedings of Fast '91, First International Conference on Fast Sea Transportation, Trondheim, June 1991

[2] Tulin, M.P., "Supercavitating Flows - Small Perturbation Theory," *J. of Ship Research,* Vol. 7, No. 3, Jan., 1964, pp.16-37.

[3] Geurst, J.A., "Linearized Theory of Two Dimensional Cavitating Lifting Flow," Ph.D. Thesis, Delft Technical Institute, The Netherlands, 1961.

[4] Wu, T. Y., "Inviscid Cavity and Wake Flows," Basic Developments in Fluid Dynamics, Vol. 2, Academic Press Inc., New York, 1968.

[5] Golden, D.W., "A Numerical Method for Two Dimensional, Cavitating, Lifting Bodies," S.M. Thesis, Department of Ocean Engineering, M.I.T., 1975.

[6] Jiang, C.W., "Experimental and Theoretical Investigation of Unsteady Supercavitating Hydrofoils of Finite Span," Ph.D Thesis, Department of Ocean Engineering, M.I.T., Cambridge, Mass., 1977.

[7] Lee, C.-S., "Prediction of Steady and Unsteady Performance of Marine Propellers with or without Cavitation by Numerical Lifting Surface Theory," Ph.D. Thesis, Department of Ocean Engineering, M.I.T., Cambridge, Mass., 1979.

[8] Uhlman, J.S., The Surface Singularity Method Applied to Partially Cavitating Hydrofoils," *J. of Ship Research,* Vol. 31, No. 2, June, 1987, pp. 107-124.

[9] Uhlman, J.S., The Surface Singularity or Boundary Integral Method Applied to Supercavitating Hydrofoils," *J. of Ship Research,* Vol. 33, No. 1, March 1989, pp. 16-20

[10] Lee, C.-S., "A Potential-Based Panel Method for the Analysis of a 2-Dimensional Partially Cavitating Hydrofoil," *J. of SNAK,* Vol. 26, No. 4, Dec., 1989, (in Korean), pp. 27-34.

[11] Lee, C.-S., Kim, Y.-G., Lee, J.-T., "A Potential-Based Panel Method for the Analysis of a Two Dimensional Super- or Partially Cavitating Hydrofoil," *J. of Ship Research,* Vol. 36, No. 2, June 1992, pp. 168-181.

[12] Kim, Y.-G., Lee, C.-S., Lee, J.-T., "A Potential-Based Panel Method for the Analysis of a Two Dimensional Super-Cavitating Hydrofoil," SNAK Autumn meeting, 1990; also available in *J. of SNAK,* Vol. 28, No. 2, Oct. 1991, pp. 159-173 (in Korean).

[13] Kinnas, S.A., Fine, N.E., "Nonlinear Analysis of the Flow Around Partially or Super-Cavitating Hydrofoils by a Potential Based Panel Method," IABEM-90 of the International Association for Boundary Element Method, 1990.

[14] Street, R.L., "A note on Gravity Effects in Supercavitating Flow," *J. of Ship Research,* Vol. 8, No. 4, March, 1965, pp. 39-46.

[15] Street, R.L., "Supercavitating Flow About a Slender Wedge in a Transverse Gravity Field," *J. of Ship Research,* Vol. 7, No. 1, June, 1963, pp. 14-24.

[16] Kiceniuk, T., Acosta, A.J., "Experiments on Gravity Effects in Supercavitating Flow," *J. of Ship Research,* Vol. 10, June, 1966, pp. 119-121.

[17] Larock, B.E., Street, R.L., "A nonlinear theory for a fully cavitating hydrofoil in a transverse gravity field," *J. of Fluid Mechanics,* Vol. 29, 1967, pp. 317-336.

[18] Yim, B., "On a fully cavitating two-dimensional flat plate hydrofoil with nonzero cavitation number near a free surface," *Hydronautics, Tech. Rep.* no. 463-4, Laurel, Md, 1964.

[19] Green, T. III, Street, R.L., "Two Supercavitating Hydrofoils Near a Free Surface," *J. of Fluid Mechanics,* Vol. 27, 1967, pp. 1-28.

[20] Larock, B.E., Street, R.L., "A Nonlinear Solution for a Fully Cavitating Hydrofoil Beneath a Free Surface," *J. of Ship Research,* Vol. 11, No. 2, June, 1967, pp. 131-139.

[21] Furuya, O., "Nonlinear calculation of arbitrarily shaped supercavitating hydrofoils near a free surface," *J. of Fluid Mechanics,* Vol. 68, 1975, pp.21-40.

[22] Doctors, L.J., "Effects of a Finite Froude Number on a Supercavitating Hydrofoil," *J. of Ship Research,* Vol. 30, No. 1, March, 1986, pp. 1-11.

[23] Wu, T. Y., "Cavity and Wake Flows," Annual Review of Fluid Mechanics, Vol. 4, 1972, pp. 243-284.

[24] Bai, K.J., " A Localized Finite-Element Method for Two-Dimensional Steady Potential Flows with a Free Surface," *J. of Ship Research,* Vol. 22, No. 4, Dec. 1978, pp. 216-230.

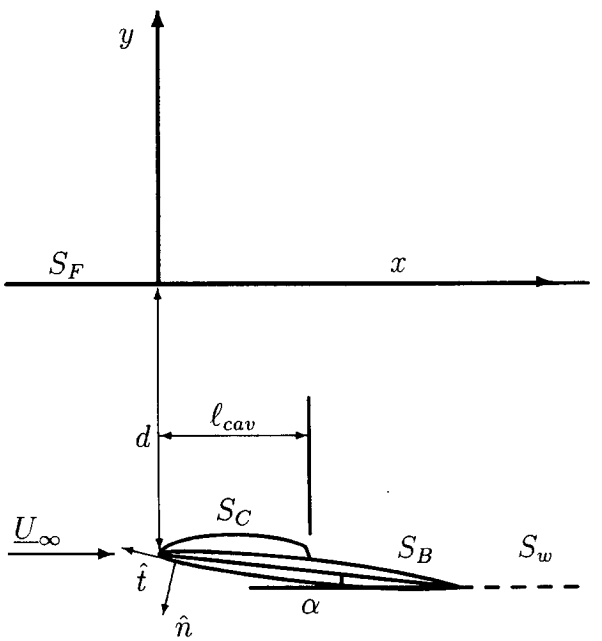

Figure 1: Coordinate system and definition sketch of a cavitating hydrofoil.

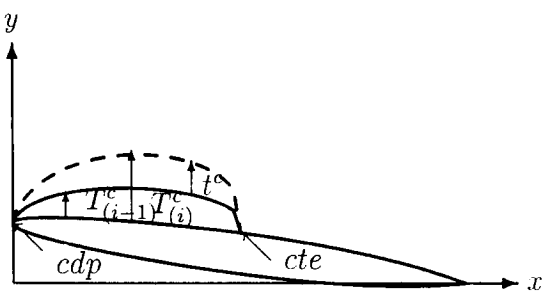

Figure 2: Definition sketch of the cavity surface position at each iteration.

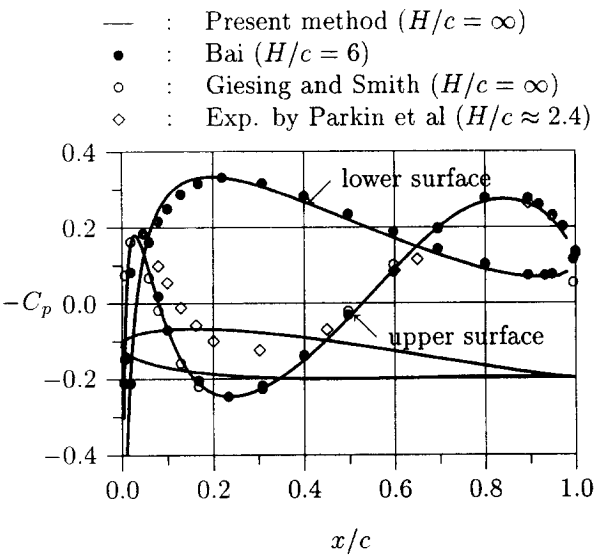

Figure 3: Pressure distribution on a 12% thick Joukowski hydrofoil at $\alpha = 5$ deg, $F_c = 0.617$, and the leading edge submergence $d/c = 0.113$. Fluid depth, H, is infinite. Data taken from Bai[24].

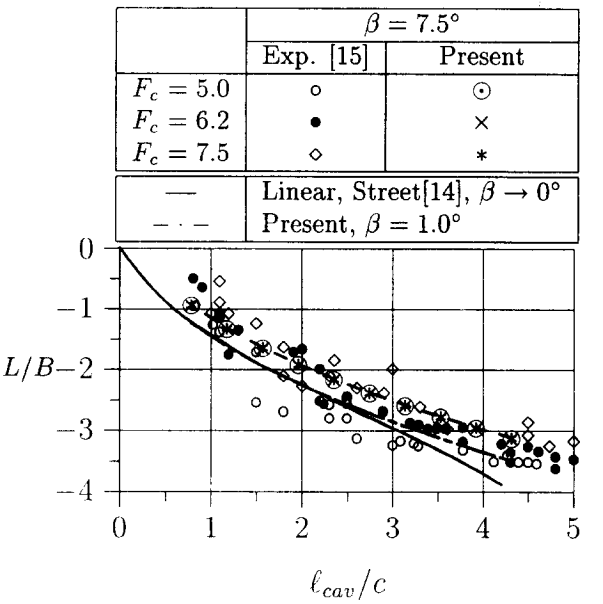

Figure 4: Ratio of the buoyancy induced lift to the displaced weight of the wedge versus the cavity length for $\beta = 7.5$ deg. Comparison with the linear theory of Street[14] and experiments of Kiceniuk and Acosta[16].

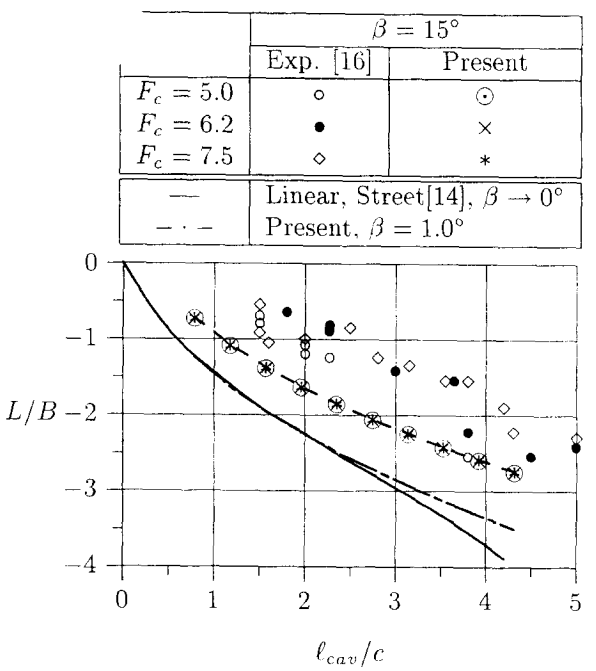

Figure 5: Ratio of the buoyancy induced lift to the displaced weight of the wedge versus the cavity length for $\beta = 15$ deg.

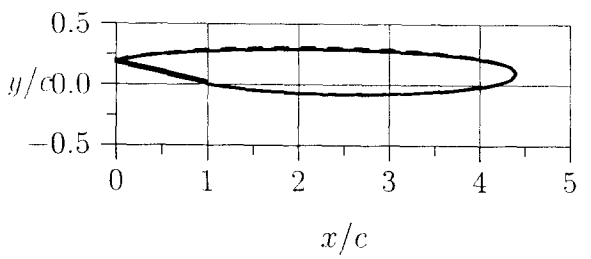

Figure 6: Effect of the transverse gravity field upon the cavity shape on a supercavitating flat-plate hydrofoil at $\alpha = 10$ deg, $F_c = 4.0$ and $d/c = \infty$; Predicted with(——) and without(– – –) the hydrostatic pressure.

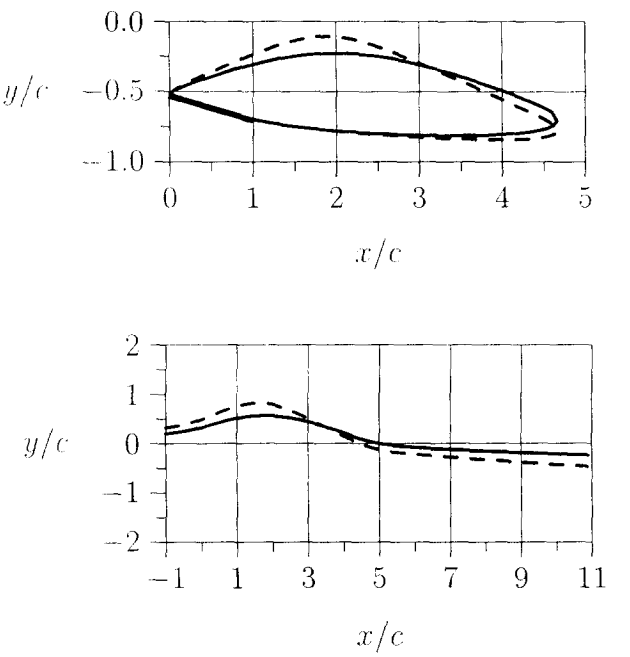

Figure 7: Effect of the transverse gravity field upon the cavity shape(above) and wave profile(below) past a supercavitating flat-plate hydrofoil at $\alpha = 10$ deg, $F_c = 4.0$ and $d/c = 0.53$; Predicted with(——) and without(– – –) the hydrostatic pressure term.

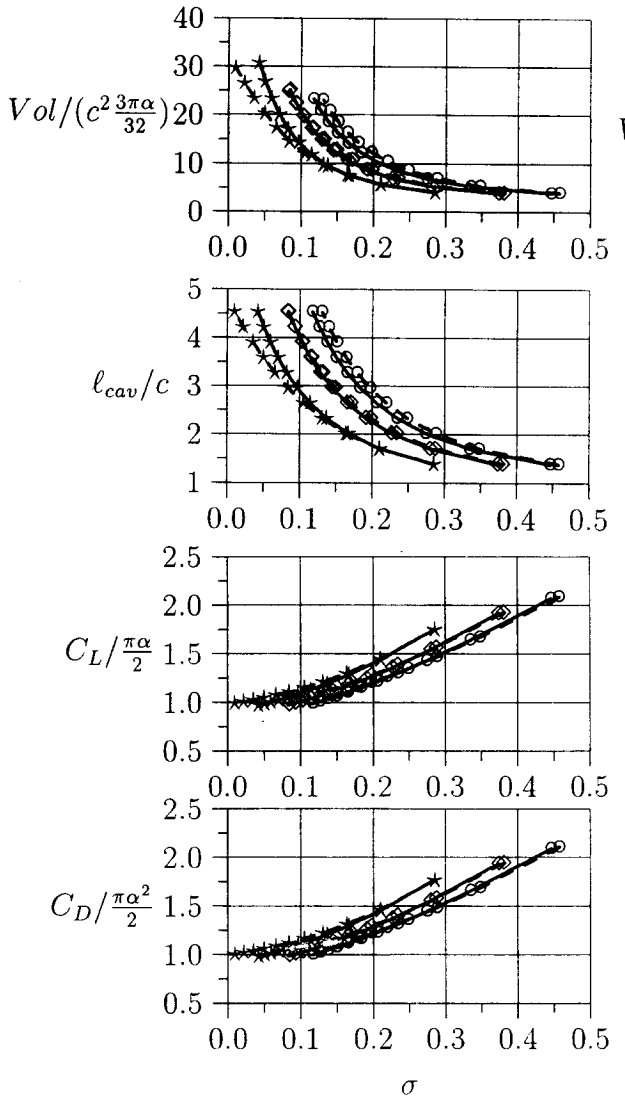

Figure 8: Effect of the transverse gravity field upon the cavity volume, the cavity length, the lift coefficient and the drag coefficient for a supercavitating hydrofoil at $\alpha = 10$ deg, $F_c = 3.0$, for three submergence depths, $d/c = 0.5(\star), 1.0(\diamond)$ and $2.0(\circ)$; Predicted with(——) and without(– – –) the buoyancy effect.

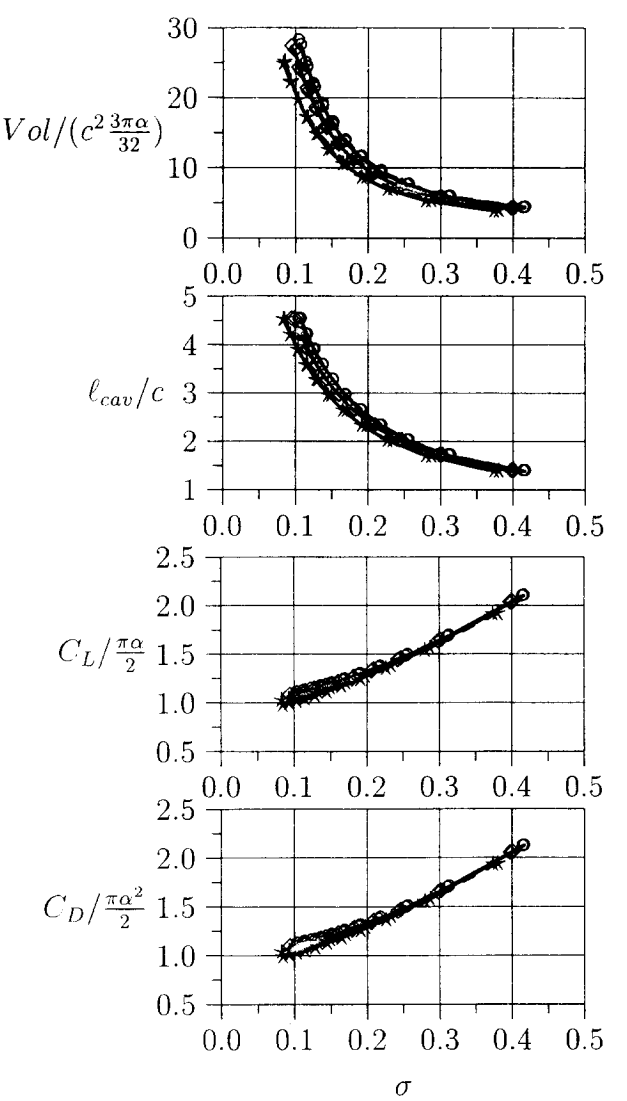

Figure 9: Effect of the transverse gravity field upon the cavity volume, the cavity length, the lift coefficient and the drag coefficient for a supercavitating hydrofoil at $\alpha = 10$ deg, $d/c = 1.0$, for three Froude numbers, $F_c = 3.0(\star), 4.0(\diamond)$ and $5.0(\circ)$; Predicted with(——) and without(– – –) the buoyancy effect.

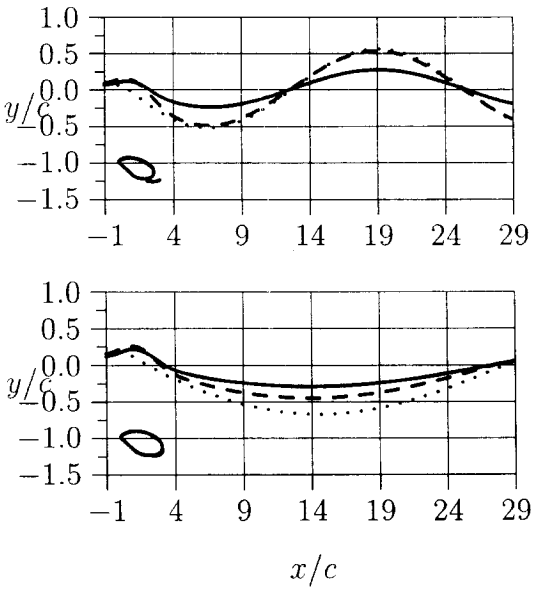

Figure 10: Buoyancy effect upon the cavity and wave profiles past a supercavitating flat-plate hydrofoil at $\alpha = 10$ deg, $d/c = 1.0$ for two Froude numbers, $F_c = 2.0$(upper) and 3.0(lower); Predicted with(——) and without(− − −) the buoyancy effect. Non-cavitating case(·····) is added for comparison.

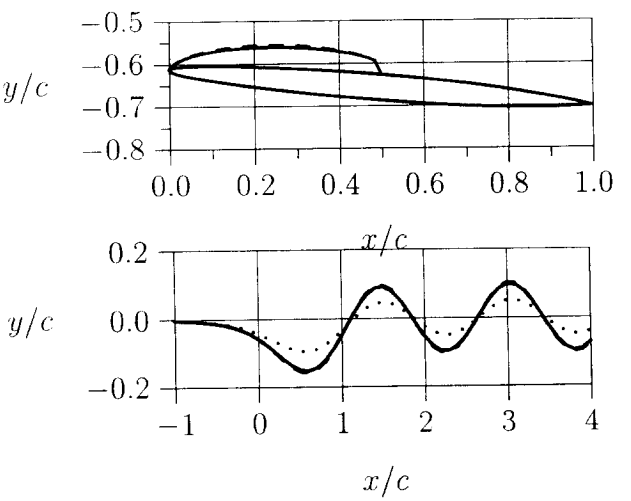

Figure 11: Effect of the transverse gravity field upon the cavity shape and the wave profile past a partially cavitating hydrofoil with NACA 16-006 section at $d/c = 0.6$, $\alpha = 5$ deg and $F_c = 0.5$, for a cavity length, $\ell_{cav}/c = 0.5$. The cavity and wave profiles predicted with(——) and without(− − −) the hydrostatic pressure term are not distinguishable. Non-cavitating case (· · · · ·) is added for comparison. $N^D = 200$.